Biophysical Journal
Article

Biophysical Society

Gating Currents in the Hv1 Proton Channel

Victor De La Rosa[1] and Ian Scott Ramsey[1,*]
[1]Department of Physiology and Biophysics, School of Medicine, Virginia Commonwealth University, Richmond, Virginia

ABSTRACT The Hv1 proton channel shares striking structural homology with fourth transmembrane helical segment-type voltage-sensor (VS) domains but manifests distinctive functional properties, including a proton-selective "aqueous" conductance and allosteric control of voltage-dependent gating by changes in the transmembrane pH gradient. The mechanisms responsible for Hv1's functional properties remain poorly understood, in part because methods for measuring gating currents that directly report VS activation have not yet been described. Here, we describe an approach that allows robust and reproducible measurement of gating-associated charge movements in Hv1. Gating currents reveal that VS activation and proton-selective aqueous conductance opening are thermodynamically distinct steps in the Hv1 activation pathway and show that pH changes directly alter VS activation. The availability of an assay for gating currents in Hv1 may aid future efforts to elucidate the molecular mechanisms of gating cooperativity, pH-dependent modulation, and H^+ selectivity in a model VS domain protein.

INTRODUCTION

The voltage-gated proton channel Hv1 is a member of a large superfamily of voltage-sensor- (VS) domain-containing proteins that function as voltage-gated ion channels (VGCs) and voltage-sensitive lipid phosphatases (VSPs) (1–4). Despite lacking a canonical ion-channel-pore domain, Hv1 mediates an activated-state H^+-selective "aqueous" conductance (G_{AQ}) that is believed to utilize a water-wire pathway for H^+ transfer within the hydrated VS-domain central crevice (1,2,5–9). Although residues that alter ion selectivity in Hv1 have been identified (10,11), it remains unclear why G_{AQ} is observed in Hv1 but not related VS domains (5,6). New methods that isolate VS activation from G_{AQ} opening are therefore needed.

A generally accepted model of VS activation posits that changes in membrane potential act on gating charges to drive conformational rearrangement of the fourth transmembrane helical segment (S4) in the VS domain (12). The phenomenological similarities between time- and voltage-dependent gating in dimeric Hv1 channels and the gating of cation currents through the pore domains of tetrameric VGCs strongly suggest that VS activation operates by a similar mechanism (1,2,9,13–15). However, Hv1 also manifests biophysical features, such as allosteric control of voltage-dependent gating by changes in the transmembrane pH gradient ($\Delta pH = pH_I - pH_O$), that are evidently unique among VGCs and VSPs (1,2,7,9,16,17). The structural and mechanistic bases for functional differences between Hv1 and related VS-domain-containing proteins are incompletely understood.

In VGCs and VSPs, depolarization-dependent S4 movement reorganizes protein-associated charges within the electrical field, producing a capacitive gating-associated current (I_G) that is integrated in time to yield the total "on" gating charge (Q_{ON}) (18). Under appropriate experimental conditions (i.e., when permeant ions are removed or an inactivating pore mutation is introduced), I_G can be directly measured using voltage-clamp electrophysiology (18–20). In VGCs, the shapes and positions of the gating charge versus voltage (Q-V) and conductance versus voltage (G-V) relations are different, indicating that they represent thermodynamically distinct events in the channel activation pathway (18,21). Studies have begun to elucidate the molecular mechanisms of "electromechanical" coupling in tetrameric VGCs (21–25), but it remains unclear whether a similar phenomenon occurs in Hv1 channels. To directly address this question, gating current measurements are needed. However, the intrinsic G_{AQ}-mediated H^+ current in Hv1 is likely to confound efforts to record I_G in isolation.

Compared to ionic currents, gating-current amplitudes are small; removal of the permeant ion or pore block thus

Submitted April 2, 2018, and accepted for publication April 30, 2018.

*Correspondence: isramsey@vcu.edu

Victor De La Rosa's present address is Department of Cell and Integrative Physiology, University of Texas Health Science Center at San Antonio, San Antonio, Texas

Editor: Baron Chanda.

https://doi.org/10.1016/j.bpj.2018.04.049

© 2018 Biophysical Society.

serves to reduce or eliminate ionic current and experimentally isolate I_G (18–20). Abolishing G_{AQ}-mediated current in Hv1 by ion substitution would likely require that the recording-solution pH be raised (i.e., $[H^+]$ lowered) beyond the range that is permissive for voltage-clamp electrophysiology in biological membranes, limiting the utility of this approach. N214R (N4R) and N214K substitutions were previously shown to attenuate steady-state outward currents carried by G_{AQ}, but inward "tail" currents (I_{TAIL}) remain measurable (7,9,26). Introducing N4R into the background of R205H (R1H) permits isolation of the resting-state H^+ "shuttle" conductance (G_{SH}) without substantially perturbing G_{AQ} gating (9), suggesting that N214R could also be useful for revealing I_G in Hv1. Here, we show that incorporating N214R into the background of rapidly activating Hv1 mutants (W207A or R205A) enables direct measurement of gating currents in human Hv1 channels expressed in mammalian cells.

MATERIALS AND METHODS

Cell culture and electrophysiology

Wild-type (WT) or mutant human Hv1 cDNA (NM_032369) in the pcDNA5/FRT/TO vector was used to create isogenic tetracycline-inducible FlpIn293-TREx stable cell lines as previously described (9). Cells were plated onto glass coverslips, and expression of mutant Hv1 proteins was induced by addition of tetracycline (1.0 μg/mL) to the culture medium 24–72 h before electrophysiology. Whole-cell currents were measured at 22–24°C using an A-M Systems model 2400 amplifier (A-M Systems, Sequim, WA) as described previously (9). Currents are elicited by voltage-step protocols from a holding potential (V_{HOLD}) to the prepulse step potential (V_{STEP}) for the indicated time and subsequently to the test potential (V_{TEST}; typically +100 mV). Data were low-pass filtered at 2–5 kHz and digitized at 10–20 kHz using a National Instruments USB-5251 DAQ (National Instruments, Austin, TX) interfaced to a PC computer running a custom LabVIEW 7-based data acquisition and amplifier control program (C. A. Villalba-Galea; details and software distribution available on request). Data were analyzed using Clampfit9 (Molecular Devices, San Jose, CA) and Origin 8.1 (OriginLab, Northampton, MA). The standard intracellular and extracellular solutions contained the following (in mM): 100 Bis (2-hydroxyethyl)amino-tris(hydroxymethyl) methane (Bis-Tris), 1 ethylene glycol tetraacetic acid (EGTA), and 8 HCl; pH was adjusted to 6.5 and a final osmolality of 310–320 mOsm by the addition of tetramethylammonium hydroxide (TMAOH) and methanesulfonic acid ($HMeSO_3$). pH_O-dependent gating was measured in bath solutions containing 100 mM 2-(*N*-morpholino)ethanesulfonic acid (MES, pH 5.5) in place of Bis-Tris, as previously described (7). Series resistance is routinely compensated ~80%, and liquid-junction potential corrections are not applied.

Data analysis

Unless otherwise indicated, data represent means ± standard error (SE) of values measured in *n* cells. I_{STEP} represents the peak current during steps to the indicated potential (V_{STEP}). The activated state "aqueous" conductance in Hv1 (G_{AQ}) was calculated from $G_{AQ} = I_{STEP}/V\text{-}E_{REV}$, where E_{REV} is the zero-current potential determined from inspection of the I_{STEP}-V relation. Tail current (I_{TAIL}) amplitude is measured by fitting the decaying current to a monoexponential function of the form $I_{TAIL} = I_0 + Ae^{-V/t}$ (where I_0 is the minimal current after decay of I_{TAIL}, A is current amplitude, V is membrane potential, and *t* is time) and extrapolating fits to the instant the voltage was changed. Leak currents were subjected to offline linear subtraction. To estimate voltage-dependent gating parameters, I_{TAIL}-V relations are fitted to a Boltzmann function of the following form: $I_{TAIL} = \left((I_{TAIL\ max}) - (I_{TAIL\ min})/1 + e^{V-V_{0.5}}/dx\right) + I_{TAIL\ min}$, where $V_{0.5}$ is the voltage at which 50% of the maximal current is reached, *dx* is a slope factor, and $I_{TAIL\ max}$ and $I_{TAIL\ min}$ represent the maximal and minimal tail-current amplitudes, respectively. G_{AQ}-V relations are fitted to a single Boltzmann of the form $G_{AQ} = \left((G_{AQmax}) - (G_{AQmin})/1 + e^{V-V_{0.5}}/dx\right) + G_{AQ_{min}}$, where $V_{0.5}$, *dx*, $G_{AQ\ max}$, and $G_{AQ\ min}$ have the same meanings as defined for I_{TAIL}. In some cases, effective gating valence (z_G) was calculated from Boltzmann fits, where $z_G = RT/F \times dx$, where F, R, and T have their usual meanings (i.e., RT/F = 25.3 mV at 20°C, the approximate temperature at which experiments were conducted). Curve fits reported in figure legends represent the best fit to the mean data; Table 1 reports mean ± SE of fitted or calculated values determined separately in the indicated number of individual experiments.

The G_{AQ} activation time course (see Fig. 1, *A* and *B*) is fitted to a single exponential function of the form $I = I_{max}\left(1 - e^{-(t-d)/\tau}\right)$, where *I* is the measured I_{TAIL} at time *t* and I_{max} is I_{TAIL} at $t = \infty$, *d* is the delay, and τ is the activation time constant (i.e., τ_{ACT}). G_{AQ} activation in W207A-N214R-ΔC (see Fig. S3) is fitted to a monoexponential function of the form $I_{TAIL} = I_{TAIL\ max}\left(1 - e^{-(t)/\tau}\right)$. The fitted exponential time course is then scaled to the amplitude of the steady-state I_{STEP} at each voltage (i.e., $I_{TAIL\ max} = I_{STEP}$) and subtracted from the measured I_{STEP} to yield transient outward I_G at each V_{STEP}. Channel number (N) is calculated by dividing the total gating charge (Q_{ON}) by the unitary gating valences ($z\delta = 6\ e_0$ for full-length Hv1 channels and $z\delta = 3\ e_0$ for ΔC truncated channels) estimated from variance analysis (27). Unitary conductance (γ_{AQ}) is calculated from the slope of a plot of $G_{AQ\ max}$ (determined from I_{TAIL}) versus N (i.e., $G_{AQ\ max} = N \times \gamma_{AQ}$). The "on" gating charge (Q_{ON}) is determined by the trapezoidal integration of I_G.

TABLE 1 Fitted and Calculated Gating Parameters

		Q_{ON}			I_{TAIL}			I_{TAIL}-Q_{ON}
Construct	Parameter	Mean	SE	*n*	Mean	SE	*n*	Difference
W207A-N214R	V_M (mV)	−38.9	0.8	6	−31.6	0.8	6	7.3[a]
	$V_{0.5}$ (mV)	−40.0	1.1	6	−31.4	0.6	6	8.6[b]
	z_G (e_0)	2.80	0.06	6	3.21	0.11	6	0.41^{NS}
W207A-N214R-ΔC	V_M (mV)	−24.1	0.3	12	−11.3	0.4	12	12.8[c]
	$V_{0.5}$ (mV)	−24.6	0.3	12	−15.7	0.4	12	8.9[d]
	z_G (e_0)	1.75[e]	0.01	12	1.52[f]	0.02	12	−0.23[g]
R205A-N214R	V_M (mV)	17.8	0.8	3	25.7	1.6	3	8.0^{NS}
	$V_{0.5}$ (mV)	25.1	2.3	3	26.4	1.3	3	1.3^{NS}
	z_G (e_0)	2.14[h]	0.12	3	1.89[i]	0.07	3	-0.25^{NS}

Data represent calculated V_M or Boltzmann-fitted $V_{0.5}$ and $z\delta$ parameters for Q_{ON}-V and I_{TAIL}-V relations measured at pH_O 6.5 in the indicated number of cells.
[a]W207A-N214R: I_{TAIL} V_M vs. Q_{ON} V_M, $p = 0.03$.
[b]W207A-N214R: I_{TAIL} $V_{0.5}$ vs. Q_{ON} $V_{0.5}$, $p = 0.02$.
[c]W207A-N214R-ΔC: I_{TAIL} V_M vs. Q_{ON} V_M, $p = 1.6 \times 10^{-7}$.
[d]W207A-N214R-ΔC: I_{TAIL} $V_{0.5}$ vs. Q_{ON} $V_{0.5}$, $p = 2.2 \times 10^{-5}$.
[e]Q_{ON} z_G: W207A-N214R vs. W207A-N214R-ΔC, $p = 2.3 \times 10^{-7}$.
[f]I_{TAIL} z_G: W207A-N214R vs. W207A-N214R-ΔC, $p = 5.6 \times 10^{-7}$.
[g]W207A-N214R-ΔC: I_{TAIL} z_G vs. Q_{ON} z_G, $p = 0.01$.
[h]Q_{ON} z_G: W207A-N214R vs. R205A-N214R, $p = 0.01$.
[i]I_{TAIL} z_G: W207A-N214R vs. R205A-N214R, $p = 0.02$.

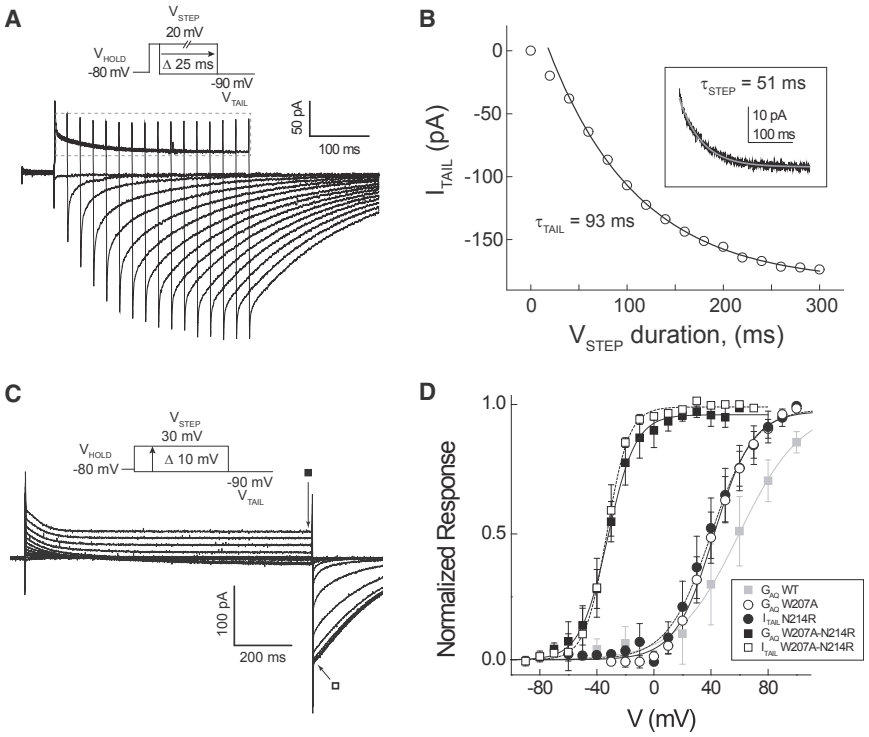

FIGURE 1 G_{AQ}-V and I_{TAIL}-V relations in Hv1 W207A-N214R. (*A*) Representative currents elicited by the indicated voltage step protocol (*inset*: $V_{HOLD} = -80$ mV; $V_{STEP} = +20$, 0–300 ms duration in 25 ms increments; $V_{TAIL} = -90$ mV) in a cell expressing in W207A-N214R are shown. Current measured during the 300-ms-duration V_{STEP} is magnified in (*B, inset*). (*B*) I_{TAIL} amplitude (current shown in (*C*)) is plotted as a function of V_{STEP} duration. The solid black line represents a fit of the data to a single exponential decay function ($\tau_{TAIL} = 93$ ms) after a delay (18 ms). The inset shows current elicited by $V_{STEP} = +20$ mV, duration 300 ms; the solid gray line represents a fit of the data to a single exponential decay function ($\tau_{STEP} = 51$ ms). (*C*) Representative currents elicited by the indicated voltage protocol (*inset*: $V_{HOLD} = -80$ mV; $V_{STEP} = -90$ to $+30$ mV in 10-mV increments, 1-s duration; $V_{TAIL} = -90$ mV) in a cell expressing W207A-N214R are shown. Symbols indicate times at which I_{STEP} (*filled square*) and I_{TAIL} (*open square*) are measured. (*D*) Steady-state currents measured at the end of V_{STEP} (I_{STEP}) are used to calculate G_{AQ} (see Materials and Methods), and data are normalized to their respective maxima in each cell to generate G_{AQ}-V relations for WT (*filled gray squares*; $n = 4$), W207A (*open circles*; $n = 4$), and W207A-N214R (*filled squares*; $n = 7$). Mean normalized I_{TAIL}-V relations are shown for N214R (*filled circles*; $n = 4$) and W207A-N214R (*open squares*; n = 9). Solid lines indicate Boltzmann fits to the mean G_{AQ}-V (WT, *gray line*: $V_{0.5} = +59.7$ mV, $z_G = 1.2\ e_0$; W207A: $V_{0.5} = +41.9$ mV, $z_G = 1.9\ e_0$; W207A-N214R: $V_{0.5} = -32.3$ mV, $z_G = 2.6\ e_0$) and dashed lines indicate Boltzmann fits to mean I_{TAIL}-V (N214R: $V_{0.5} = +40.1$ mV, $z_G = 1.7\ e_0$; W207A-N214R: $V_{0.5} = -33.0$ mV, $z_G = 3.3\ e_0$) relations.

Requests for biological materials (i.e., cDNA constructs used for this study) should be directed to the corresponding author. Additional information and requests for software used for integration of gating currents may be directed to Carlos A. Villalba-Galea (cvillalbagalea@pacific.edu).

RESULTS

To measure gating-charge movement in Hv1, we hypothesized that it would be necessary to identify a mutant channel in which 1) the time course of G_{AQ} activation is greatly accelerated and 2) current carried by G_{AQ} is greatly diminished. A mutation of a conserved Trp residue in the S4 helix of Hv1 (W207) is reported to greatly speed the time course of G_{AQ} activation (28). Mutations at R205 (R1) also exhibit rapid G_{AQ} activation by membrane depolarization (1,2,7,9,27,29), but the effects of this and other S4 Arg mutations to decrease the apparent gating-charge valence (z_G) (27) represent a potential limitation for their use in measuring gating current. Introducing an additional Arg residue into the S4 helix of Hv1 (N214R) was previously shown to block outward steady-state currents carried by G_{AQ} (7,9,26). We therefore combined W207A and N214R mutations (W207A-N214R) and induced expression of mutant channels in a modified HEK-293 cell line by addition of tetracycline to the culture medium (see Materials and Methods).

W207A-N214R alters G_{AQ} activation kinetics and steady-state voltage-dependent gating

We previously reported that nontransfected cells and cells that were not exposed to tetracycline do not exhibit voltage-dependent currents under the recording conditions used here (7). However, robust voltage-gated currents are measured under whole-cell voltage clamp in cells expressing N-terminally tagged EGFP-hHv1 W207A-N214R (Fig. 1 *A*). Increasing the duration of the voltage step (V_{STEP}) to $+20$ mV causes the amplitude of the subsequent, inwardly directed tail current (I_{TAIL}) measured at -90 mV to increase and eventually plateau (Fig. 1, *A* and *B*). Peak I_{TAIL} rises sigmoidally with V_{STEP} duration and is fitted to a single-exponential function after a delay (Fig. 1 *B*), similar to WT Hv1 channels (1,2,28,30). The fitted time constant for I_{TAIL} activation ($\tau_{TAIL} = 93$ ms) is substantially faster than WT Hv1 but slower than W207A (28). Unlike W207A and WT Hv1, which pass outward G_{AQ}-mediated currents that display sigmoid activation kinetics during a fixed voltage step (1,2,28), W207A-N214R exhibits a complex biphasic time course (Fig. 1 *A*). A rapidly activating transient outward current decays to an apparent steady state with a fitted time course ($\tau_{STEP} = 51$ ms) that is almost two times faster than I_{TAIL} (Fig. 1 *B*). The kinetic difference between I_{STEP} and I_{TAIL} activation time courses suggests that

the transient-current decay may report a conformational change that precedes the opening of G_{AQ}.

Next, we sought to establish experimental conditions under which I_G and I_{TAIL} are measured under apparent steady-state conditions. Q_{ON} and I_{TAIL} are each time and voltage dependent (Fig. S1, *A–D*), and Boltzmann fits to the data show that the fitted $V_{0.5}$ and slope factors (apparent z_G) also depend on the duration of the preceding voltage step (Fig. S1, *E* and *F*). A voltage step (V_{STEP}, before I_{TAIL} measurement) or prepulse (V_{PP}, before Q_{ON} measurement) of 1-s duration is evidently sufficient to achieve apparent equilibrium conditions, because a longer voltage pulse elicits no additional changes in either the fitted $V_{0.5}$ or z_G (Fig. S1, *E* and *F*). We therefore measure I_{STEP} at the end of a 1-s depolarization and calculate conductance to determine the G_{AQ}-V relation; I_{TAIL} is measured after a subsequent hyperpolarizing step as described previously (1,9).

As expected, the I_{TAIL}-V and G_{AQ}-V relations in W207A-N214R are highly similar, indicating that they report the same conformational transition, namely, G_{AQ} activation. Compared to WT Hv1 and W207A and N214R single mutants, G_{AQ} gating is shifted toward negative potentials in W207A-N214R (Fig. 1 *D*). The fitted midpoint ($V_{0.5}$) of the G_{AQ}-V and I_{TAIL}-V relations in W207A-N214R are ~90 mV more negative than WT Hv1 and ~70 mV more negative than either W207A or N214R (Fig. 1 *D*). Interestingly, the slopes of Boltzmann fits to the G_{AQ}-V and I_{TAIL}-V relations are shallower in WT Hv1 than in W207A, N214R, or W207A-N214R mutant channels (Fig. 1 *D*). The similarity in z_G calculated from Boltzmann fits suggests that the kinetically fast mutant channels tested here are likely to move a similar quantity of gating charge during VS activation. Although measurement of the limiting slope suggests that $z_G = \sim 6\ e_0$ in WT *Ciona intestinalis* Hv1, indicating that G_{AQ}-V and I_{TAIL}-V relations may significantly underestimate z_G (27), z_G estimates in mutant channels measured here may nonetheless be usefully compared (Table 1).

Gating currents in Hv1 W207A-N214R

Because G_{AQ} is not substantially open at early times after depolarization, we hypothesize that rapidly activating transient outward currents could represent I_G in Hv1. As in WT Hv1, the kinetics of G_{AQ} opening in W207A-N214R are both time and voltage dependent (Fig. S1, *A* and *B*). The decay of the transient outward current measured at various potentials is also evidently voltage dependent (Fig. 2 *A*). Although it should be possible to subtract the G_{AQ}-mediated component of current from the aggregate I_{STEP} to yield I_G in isolation (Fig. 1, *A* and *B*), the time course of G_{AQ} activation follows a complex sigmoidal time course (31). Determining the amplitude of H^+-current I_{STEP} contributed by G_{AQ} at each time and voltage depends on accurate kinetic modeling of the activation pathway, which is impractical in W207A-N214R because outward H^+ currents are blocked. Instead, we opt to record transient outward currents at a fixed potential (i.e., $V_{STEP} = +100$ mV) after stepping through a range of prepulse voltages (V_{PP}). A step to +100 mV from a large

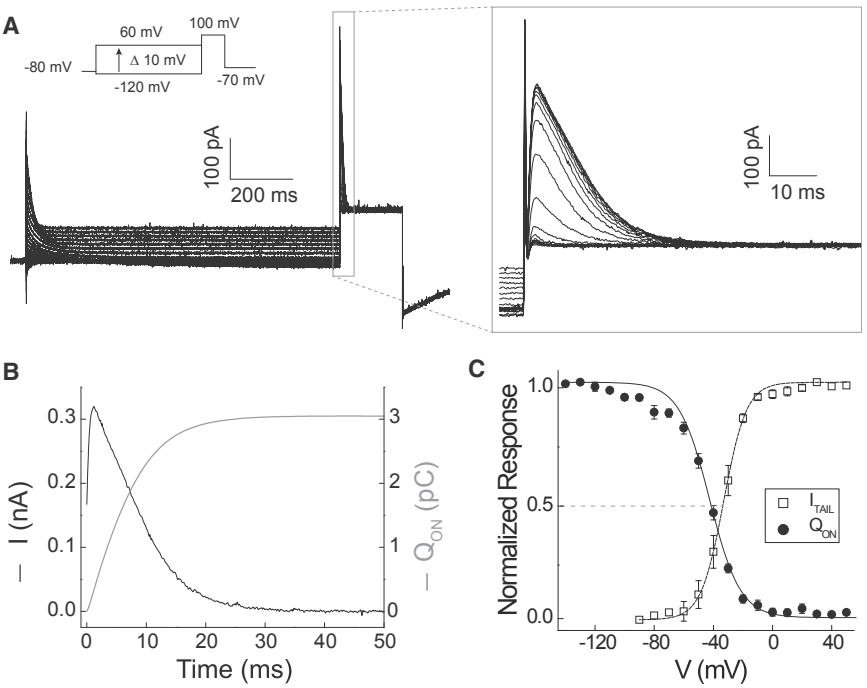

FIGURE 2 Integration of transient outward current reveals "on" gating charge (Q_{ON}) movement. (*A*) Representative currents elicited by the indicated voltage protocol ($V_{HOLD} = -80$ mV; $V_{PP} = -120$ to +60 mV in 10-mV increments, 1-s duration; $V_{STEP} = +100$ mV, 200-ms duration; $V_{TAIL} = -70$ mV) are shown. Transient outward currents at $V_{STEP} = +100$ mV within the dashed box are magnified in the boxed inset. Steady-state currents measured at the end of V_{PP} are attributed to G_{AQ} (see also Figs. S3 and S4). (*B*) The transient outward current ($V_{PP} = -100$ mV, $V_{STEP} = +100$ mV, *black line*) is plotted together with its time integral (Q_{ON}, *gray line*). The timescale is adjusted to reflect the rise in transient outward current after a brief initial current that we attribute to uncompensated capacitance. In this example, gating current integration begins 1.75 ms after the V_{STEP} voltage command is applied. (*C*) Q_{ON} (*filled circles*) measured at $V_{STEP} = +100$ mV ($V_{PP} = -120$ mV, 1000 ms duration) is normalized to its maximum in each cell and mean data ($n = 9$ cells) are plotted in function of V_{PP}. The mean I_{TAIL}-V relation (*open* circles; data from Fig. 1 *B*) is replotted for comparison. Lines represent fits to Boltzmann functions (Q_{ON}, *solid line*: $V_{0.5} = -42.5$ mV; $z_G = 2.5\ e_0$; I_{TAIL}, *dashed line*: $V_{0.5} = -33.0$ mV, $z_G = 3.3\ e_0$). Median voltages (V_M) calculated for the normalized mean Q_{ON}-V and I_{TAIL}-V relations shown here are $V_M = -44.9$ mV and $V_M = -33.2$ mV, respectively.

negative V_{PP} (i.e., −120 mV), at which the open probability for G_{AQ} is evidently close to its minimum (Fig. 1 *D*), elicits a large transient outward current with a complex rising and falling kinetic profile (Fig. 2 *A*). The initial spike of outward current seen in Fig. 2 *A* is attributed to incomplete compensation of the membrane capacitance and is not analyzed further here. As expected, the amplitude of the transient outward current measured at +100 mV saturates at both positive and negative V_{PP} (Fig. 2 *A*), suggesting that it represents an authentic I_G in Hv1.

Integrating I_G yields a direct measure of the gating charge generated by functional Hv1 channels in the plasma membrane (Q_{ON}). As expected, Q_{ON} rises exponentially and saturates in time, as illustrated in a representative experiment in which I_{STEP} is measured at +100 mV (Fig. 2 *B*). Integrating I_{STEP} over a range of V_{PP} yields a highly nonlinear Q_{ON}-V relation that clearly saturates at large positive and negative potentials (Figs. 2 *C* and S1). Q_{ON} is maximal after V_{PP} to hyperpolarizing voltages that are expected to drive occupancy of resting-state VS conformations and Q_{ON} falls toward zero as the driving force for gating-charge translocation decreases (Figs. 2 *C* and S1). To compare I_{TAIL}-V and Q_{ON}-V gating parameters, we initially compared Boltzmann fits of the data (Fig. S1). Surprisingly, $V_{0.5}$ for the Q_{ON}-V relation is consistently 8–10 mV more negative than the I_{TAIL}-V relation (Figs. 2 *C* and S1; Table 1), suggesting that gating-charge movement and G_{AQ} opening represent thermodynamically distinct transitions in the Hv1 activation pathway.

In contrast to our expectations, the slopes of Boltzmann functions fitted to Q_{ON}-V relations are evidently shallower than I_{TAIL}-V relations (Figs. 1 *D* and 2 *C*; Table 1). Previous studies in both Hv1 and tetrameric VGCs show that Boltzmann fits to I_{TAIL}-V or G-V relations typically yield smaller estimates of z_G than limiting-slope or Q-V relations (1,2,27,32–34). Closer inspection reveals that although the I_{TAIL}-V relations are well described by single Boltzmann distributions (Fig. 1 *D*), the Q_{ON}-V relation characteristically deviates from the Boltzmann fit between −100 and −70 mV (Fig. 2 *C*). The data therefore suggest that gating-charge movement in Hv1 requires more than one transition, similar to tetrameric VGCs for which complex Q-V relations are not described by simple Boltzmann distributions and fitted-slope values often appear to underestimate z_G (14,20,21,35–38). We therefore calculated the median voltages (V_M) for Q_{ON}-V and I_{TAIL}-V relations to compare thermodynamic gating parameters in a model-independent fashion (38). Similar to $V_{0.5}$, we find that V_M is consistently ∼10 mV more negative for Q_{ON} than for I_{TAIL} (Table 1), indicating that G_{AQ} opening requires an additional gating transition.

Estimating channel number and unitary conductance from Hv1 gating currents

A straightforward expectation is that Q_{ON} and I_{TAIL} similarly depend on the number of functional channels (N) in the plasma membrane; maximal Q_{ON} ($Q_{ON\ max}$) is therefore expected to be tightly correlated with maximal I_{TAIL} amplitude ($I_{TAIL\ max}$). If $Q_{ON} = N \times z_G \times P_{ACT}$, where P_{ACT} is the probability that z_G has been moved (i.e., the VS domain is activated), and $I_{TAIL\ max} = N \times i \times P_{OPEN}$, where i is the unitary current and P_{OPEN} is the probability that G_{AQ} is open, the slope of the $Q_{ON\ max}$ vs. $I_{TAIL\ max}$ relation thus reports charge movement per "conducting unit" (i.e., $Q_{ON\ max}/I_{TAIL\ max} = z_G/i$). Consistent with expectations, the plot of $Q_{ON\ max}$ vs. $I_{TAIL\ max}$ is well fitted to a straight line with slope = 5.9 pC/nA (Fig. 3 *A*). Limiting-slope analysis of G_{AQ}-V relations provides an independent estimate of the gating valence ($z_G = 6\ e_0$/conducting unit) in WT, presumably dimeric *C. intestinalis* Hv1 channels (27), allowing us to calculate N from the $Q_{ON\ max}$ data. To accurately measure G_{AQ}, each cell must express ∼0.5 × 10^6 W207A-N214R conducting units, and Q_{ON} measurements are ideally

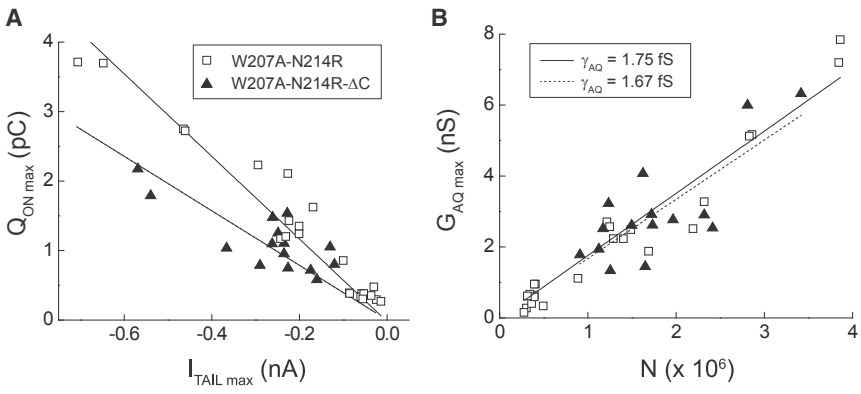

FIGURE 3 Estimating unitary conductance in Hv1 W207A-N214R. (*A*) Plots of maximal Q_{ON} ($Q_{ON\ max}$) versus maximal I_{TAIL} ($I_{TAIL\ max}$) measured in individual cells expressing W207A-N214R (*open squares*) or W207A-N214R-ΔC (*filled triangles*) are shown. Mean (± SE) $Q_{ON\ max}$ = 1.25 ± 0.22 pC, and $I_{TAIL\ max}$ = 197 ± 40 pA (n = 24 cells). Lines indicate linear fits of the data (W207A-N214, *solid line*: slope = 5.9 pC/nA; R^2 = 0.97; W207A-N214R-ΔC, *dashed line*: slope = 3.9 pC/nA; R^2 = 0.87. (*B*) The apparent number of channels (N) is calculated from the total charge ($Q_{ON\ max}$) divided by the previously reported (27) gating valences for full-length (*squares*; $z_G = 6\ e_0$) or truncated (*triangles*; $z_G = 3\ e_0$) channels' limiting-slope analyses. Linear fits of maximal G_{AQ} ($G_{AQ\ max}$) determined from Boltzmann fits to G_{AQ}-V relations in each cell (see Fig. 1 *D*) versus calculated channel number yield estimates of the G_{AQ} unitary conductances for W207A-N214R (*solid line*: γ_{AQ} = 1.75 fS) and W207A-N214R-ΔC (*dashed line*: γ_{AQ} = 1.67 fS). To see this figure in color, go online.

measured in cells that appear to express $>2 \times 10^6$ channels (Fig. 3 *B*). Using the z_G-values determined from our Boltzmann fits of Q_{ON}-V or I_{TAIL}-V relations (Table 1) would approximately double the number of channels needed to generate the measured current or charge movement. Alternatively, if z_G-values reported for *C. intestinalis* Hv1 underestimate the actual gating valence, we might overestimate N somewhat. Given that even highly similar channels like Kv1.2 and *Drosophila* Shaker can manifest dramatically different gating valences (39), some caution is warranted in the interpretation of absolute channel numbers reported here. Nonetheless, our data suggest that mutant Hv1 channels are highly overexpressed in our studies, and robust protein expression is probably an important prerequisite for I_G measurement in Hv1.

Standard ion channel theory posits that $G_{AQ\ max} = N \times \gamma_{AQ} \times P_{OPEN}$ (where P_{OPEN} is the probability of G_{AQ} being open), so γ_{AQ} can readily be calculated from the slope of the $G_{AQ\ max}$ vs. N plot (Fig. 3 *B*). Because N214R blocks G_{AQ}-mediated current by occupying a site at the intracellular entrance to the G_{AQ}-meditated H^+ transfer pathway (5,7,9,26), we calculated γ_{AQ} from I_{TAIL} measured at negative voltages at which the block is less evident. However, the estimated unitary conductance in W207A-N214R (γ_{AQ} = 1.75 fS) is still ~20-fold smaller than a previous estimate based on variance analyses of native voltage-gated H^+ currents in human eosinophils (γ = 36 fS) measured under similar experimental conditions (40). Our data are consistent with a previous study showing that N214R exerts a pronounced blocking effect on outward H^+ transfer (9) but suggest that both outward and inward H^+ currents are smaller in W207A-N214R than in WT Hv1.

Effect of mutations on gating-charge movement in Hv1

The effects of charge-neutralizing mutations indicate that conserved S4 Arg residues function as gating charges in Hv1 and other VS domain-containing proteins. We therefore combined N214R with a second-site mutation (R205A) that eliminates the most extracellular Arg in S4 (R1) and measured gating currents as described earlier. R205A-N214R exhibits rapid G_{AQ} activation kinetics, prominent G_{AQ}-mediated tail currents at negative voltages, and transient outward gating currents that are similar to W207A-N214R (Fig. S2, *A* and *B*). Although the steady-state I_{STEP} attributed to G_{AQ} appears to be larger in R205A-N214R than W207A-N214R, the G_{AQ} contribution is readily subtracted to yield transient outward currents that can be integrated to estimate Q_{ON} (Fig. S2, *A* and *C*). The positions of the R205A-N214R I_{TAIL}-V and Q_{ON}-V relations are shifted positively by ~57 mV compared to W207A-N214R, consistent with previous reports showing that S4 mutations have dramatic effects on gating kinetics and the steady-state thermodynamic properties but nonetheless retain most or all of the essential biophysical properties of voltage-gated H^+ channels (1,2,9,28). The fitted $V_{0.5}$-values for Q_{ON}-V and I_{TAIL}-V relations in R205A-N214R are not significantly different, but like in W207A-N214R, V_M-values are separated by 8 mV (Fig. S2 *C*; Table 1). z_G-values estimated from Boltzmann fits to Q_{ON}-V ($z_G = 2.1 \pm 0.1\ e_0$) and I_{TAIL}-V ($z_G = 1.9 \pm 0.1\ e_0$) relations are 0.7 e_0 and 1.3 e_0 smaller, respectively, in R205A-N214R than W207A-N214R (Table 1).

To determine whether C-terminal deletion alters z_G, we next measured gating currents in W207A-N214R-ΔC. Limiting-slope analyses indicate that z_G is ~50% smaller in Hv1-ΔC ($z_G \approx 3\ e_0$) than full-length channels, possibly because the conducting unit is a monomer rather than a dimer (14,27). If monomeric Hv1-ΔC channels function similarly to dimeric WT channels, z_G/i is not expected to be different. However, we find that the slope of the $Q_{ON\ max}/I_{TAIL\ max}$ relation is significantly smaller in W207A-N214R-ΔC than it is in full-length W207A-N214R channels (Fig. 3 *A*). We observe a similar decrease in the apparent z_G/i ratio in R205A-N214R (Fig. S2 *D*), consistent with the hypothesis that R1 neutralization decreases the total gating-charge valence (1,2,9,27). The effect of ΔC on $Q_{ON\ max}/I_{TAIL\ max}$ therefore suggests that C-terminal truncation alters a unitary channel property (z_G and/or i) in addition to its effects on dimer stability and gating cooperativity.

Using the gating valence previously determined for *C. intestinalis* Hv1-ΔC channels ($z_G = 3\ e_0$/conducting unit) (27), we estimated that the unitary conductances in W207A-N214-ΔC (γ_{AQ} = 1.67 fS) and R205A-N214R (γ_{AQ} = 2.21 fS) are not significantly different from W207A-N214R (γ_{AQ} = 1.75 fS; Figs. 3 *B* and S1 *E*). This result is consistent with an earlier study showing that the two pores in dimeric Hv1 channels are independent and each contributes equally to the total current (41). A straightforward interpretation of the data is that the reduction in $Q_{ON\ max}/I_{TAIL\ max}$ ratio, and thus z_G/i, observed in R1- and ΔC-mutant channels is mainly due to a decrease in gating valence. Consistent with this interpretation, we find that, like R205A-N214R, the Boltzmann slopes of both the Q_{ON}-V and I_{TAIL}-V relations are shallower in W207A-N214R-ΔC than in W207A-N214R (Table 1). In ΔC channels, apparent z_G from the Q_{ON}-V ($z_G = 1.8 \pm 0.1\ e_0$) and I_{TAIL}-V ($z_G = 1.5 \pm 0.1\ e_0$) are 0.9 and 1.8 e_0 smaller, respectively, than W207A-N214R (Table 1).

In addition to the effects of ΔC on steady-state properties of unitary Hv1 channels, C-terminal truncation apparently reduces complexity in the Hv1 activation pathway, as evidenced by a switch from sigmoid (WT) to exponential (ΔC) G_{AQ} activation time courses (14,26). We also find that although the time course for I_{TAIL} activation in W207A-N214R is sigmoidal (Fig. 1 *B*), I_{TAIL} evidently rises exponentially in W207A-N214R-ΔC (Fig. S3, *A*–*C*). We therefore scaled single-exponential fits of the I_{TAIL} time course to the amplitude of the current at the end of each

I_{STEP} (Fig. S3 *B*) and then subtracted the G_{AQ}-mediated component of current at each voltage from the aggregate I_{STEP}. Integrating the G_{AQ}-subtracted transient currents measured at a range of V_{STEP} yields a family of transient currents with the expected voltage and time dependence for gating current (Fig. S3 *D*). $V_{0.5}$ for the Q_{ON}-V relation in W207A-N214R-ΔC, which is well fitted to a single Boltzmann distribution, is shifted positively by ~+15 mV compared to W207A-N214R (Fig. S3 *E*; Table 1). Consistent with expectations for a gating current, the τ_{DEACT}-V relation of the G_{AQ}-subtracted transient current is bell-shaped, and the peak is located close to the fitted $V_{0.5}$ (Fig. S3, *E* and *F*). Consistent with the previously noted differences in the $Q_{ON\ max}/I_{TAIL\ max}$ relations forW207A-N214R and W207A-N214R-ΔC, we find that the mean Boltzmann slope of Q_{ON}-V relations measured at +100 mV are shallower in W207A-N214R-ΔC (z_G = 1.75 ± 0.01 e_0) than W207A-N214R (z_G = 2.80 ± 0.06 e_0, $p < 0.01$; Table 1). The mean Boltzmann slope of the W207A-N214R I_{TAIL}-V relation (z_G = 3.21 ± 0.11 e_0) is also steeper than W207A-N214R-ΔC (z_G = 1.52 ± 0.02 e_0, $p < 0.01$; Table 1). In summary, gating currents suggest that both R1 neutralization and C-terminal truncation decrease the gating valence but do not appreciably alter unitary conductance.

Gating-charge movement in W207A-N214R is sensitive to changes in pH_O

To determine whether W207A-N214R exhibits the hallmark sensitivity to changes in the pH gradient that is characteristic of Hv1 channel gating (1,2,17), we simultaneously measured I_{TAIL} and I_G at pH_O 6.5 and pH_O 5.5 (Figs. 4 *A* and S4, *A* and *B*). G_{AQ} begins to activate at voltages that are negative to the Nernst potential for H^+ (E_{H^+}), and W207A-N214R mediates steady-state inward currents that are distinct from WT Hv1 (Fig. S4, *A* and *B*). Similar to WT Hv1, however, lowering pH_O in the physiological range (i.e., $pH_O < 8$) shifts both the position of the G_{AQ}-V relation and the I_{STEP} reversal potential (ΔE_{REV} = 49.7 ± 4.1 mV, n = 5 cells; see also Fig. S4). ΔE_{REV} measured between pH_O 6.5 and pH_O 5.5 (pH_I 6.5) is close to the Nernst prediction for a H^+-selective channel (ΔE_{H+} = 56 mV at 20°C), suggesting that W207A-N214R remains reasonably H^+-selective under our recording conditions, consistent with a previous study of W207 single-mutant channels (28). As expected from the effect of extracellular acidification on the driving force for H^+ current, I_{STEP} and I_{TAIL} amplitudes are altered by pH_O changes (Fig. S4, *A* and *B*); lowering pH_O also speeds I_{TAIL} decay in W207A-N214R (Fig. S4, *A* and *B*), consistent with previous reports (1,9,17,28).

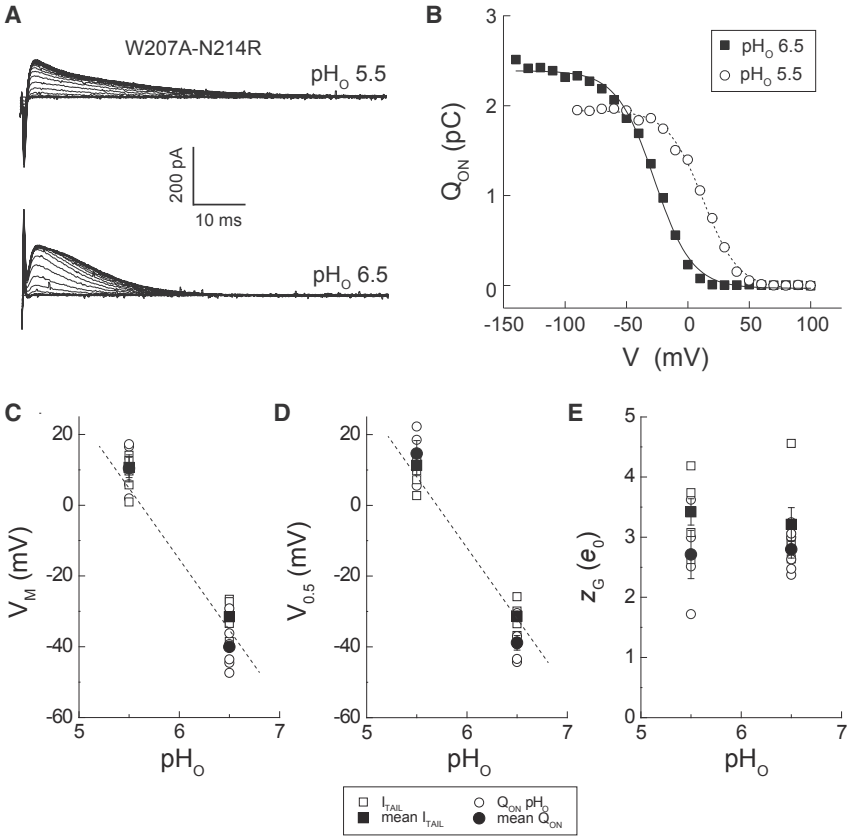

FIGURE 4 pH_O dependence of Q_{ON}-V and I_{TAIL}-V relations in W207A-N214R. (*A*) Representative outward transient current traces recorded at pH_O 5.5 (*top*) or pH_O 6.5 (*bottom*) in a cell expressing W207A-N214R are shown. Currents at +100 mV are elicited by a series of voltage steps between −140 and +100 mV (10-mV increments, duration = 200 ms; data not shown). (*B*) Representative Q_{ON}-V relations are generated by integrating the currents (data shown in (*A*): *open circles*, pH_O 5.5; *filled squares*, pH_O 6.5). Lines represent Boltzmann fits to the data (*dashed line*, pH_O 5.5: $Q_{ON\ max}$ = 1.9 pS, $V_{0.5}$ = 11.8 mV, z_G = 1.83 e_0; *solid line*, pH_O 6.5: $Q_{ON\ max}$ = 2.4 pS, $V_{0.5}$ = −27.7 mV, z_G = 1.70 e_0). (*C–E*) V_M (*C*), $V_{0.5}$ (*D*), and z_G (*E*) parameters determined for I_{TAIL}-V (*squares*) and Q_{ON}-V relations (*circles*) at pH_O 6.5 or pH_O 5.5 are shown. Mean values are indicated by filled symbols, and data from individual experiments are indicated by open symbols. Dashed lines in (*C* and *D*) indicate slope = −40 mV/pH unit. To see this figure in color, go online.

We demonstrate here for the first time, to our knowledge, that gating-charge movement in Hv1 is also pH sensitive. First, we show that the rate of I_G decay at +100 mV is faster at pH_O 6.5 compared to pH_O 5.5 (Fig. 4 *A*), indicating that the "on" gating charge moves faster at more alkaline pH. Raising pH_O reciprocally slows the time course of I_{TAIL} decay at −90 mV (Figs. 4 *A* and S4, *A* and *B*). The kinetic effects of pH_O changes on I_G and I_{TAIL} in W207A-N214R are consistent with the effect of pH_O changes on the G_{AQ} activation time course in WT Hv1, in which extracellular alkalization both speeds opening and slows closing (1,2,17,42). Consistent with the effects of pH_O changes on the G_{AQ}-V relation, $V_{0.5}$ and V_M-values determined for Q_{ON}-V relations at pH_O 6.5 and pH_O 5.5 are displaced by ~40 mV (Fig. 4, *B–D*). The magnitude of the pH-dependent shift in gating-charge movement in W207A-N214R is therefore comparable to the response measured in WT and other Hv1 mutant channels, including the W207A single mutant (7,28). In contrast to $V_{0.5}$ and V_M, z_G-values estimated from the slopes of Boltzmann fits to Q_{ON}-V and I_{TAIL}-V relations are not significantly different at pH_O 6.5 and pH_O 5.5 (Fig. 4, *B* and *E*; Table 1). Finally, we find that $Q_{ON\ max}$ is smaller at pH_O 5.5 than at pH_O 6.5 (Fig. 4 *B*). On average, the quantity of gating charge moved at pH_O 5.5 is 29% smaller than at pH_O 6.5 ($Q_{ON\ max\ pH5.5}/Q_{ON\ max\ pH\ 6.5} = 0.71 \pm 0.05$; mean ± SE, $n = 5$ cells, $p = 0.02$ by Student's paired *t*-test).

DISCUSSION

Although Hv1 shares structural and functional homology with other voltage-dependent cation channels and phosphatases, its VS domain is evidently unique in mediating an intrinsic, activated-state "aqueous" H^+ conductance (1,2,7). G_{AQ} gating in Hv1 is also strongly modulated by changes in ΔpH (1,2,17), but the molecular mechanism(s) responsible for pH-dependent gating remain unknown (7,28). Strikingly, neutralization of candidate ionizable residues in Hv1 is insufficient to abrogate either pH_O-dependent gating or H^+-selective ion permeation (5–7), but neutralization of H168 was shown to attenuate sensitivity to changes in pH_I (16). So far, only one nonfunctional mutant Hv1 channel (D112V) has been described (11), but it remains unclear whether this mutation exerts its effect by 1) causing a reorganization of the H^+ transfer pathway to block G_{AQ}-mediated H^+ transfer or 2) preventing a voltage-dependent conformational rearrangement that is necessary for G_{AQ} opening. To understand the mechanisms of VS activation and G_{AQ} gating independently from H^+ transfer, new experimental tools are needed.

Here, we show that for the first time, to our knowledge, gating currents associated with the movement of protein-associated charge can be measured in mutant Hv1 channels. We attribute the success of our experimental strategy to three factors: 1) high expression of mutant proteins driven in stable, tetracycline-inducible cell lines; 2) incorporation of mutations (W207A or R205A) that dramatically speed the normally slow G_{AQ} activation kinetics in mammalian Hv1 channels; and 3) partial block of G_{AQ}-mediated ionic current by N214R. Together, these experimental manipulations reveal the existence of transient currents with gating properties that are distinct from the ionic H^+ current. I_G directly reports VS activation, and its integral yields the quantity of charge moved, which is directly proportional to G_{AQ}. I_G measurements in the Hv1 mutants tested here exhibit all the expected features of authentic gating currents, including time- and voltage-dependent gating and saturable dependence on membrane potential. One limitation of our study is that we have so far been unable to cleanly separate the relative contributions of G_{AQ} and the "off" gating charge (Q_{OFF}) to the measured I_{TAIL}, and the expectation that $Q_{ON} = Q_{OFF}$ remains to be demonstrated. Additional studies are thus needed to identify mutant Hv1 channels in which inwardly directed H^+ currents carried by G_{AQ} are selectively blocked.

Hv1 gating currents reveal several previously unknown biophysical properties of Hv1 channels. First, the Q_{ON}-V relation is nonidentical to the G_{AQ}-V (or I_{TAIL}-V) relation, indicating that G_{AQ} opening requires a thermodynamic transition that is distinct from VS activation per se. "Electromechanical" coupling between VS activation and pore opening is a well-established phenomenon in tetrameric voltage-gated cation channels (18,21–23,25) but has not been described for Hv1, which lacks the canonical pore domain and instead utilizes the VS domain for both gating and H^+-selective ion conduction (1,2). Our results are consistent with the possibility that a conformational rearrangement that follows VS activation (i.e., the movement of gating charge in the transmembrane electrical field) is necessary to open the H^+ transfer pathway. Gating hysteresis measured in the related VSP from *C. intestinalis* (*Ci*VSP) is attributed to a voltage-independent transition (43), and evidence for a similar step in the Hv1 activation pathway has also been described previously (31). The ability to measure gating currents in Hv1 may be useful for dissecting the molecular bases of gating hysteresis and thermodynamic coupling of VS activation and G_{AQ}-mediated "gating pore" opening in a simple model protein.

The shape of the Q_{ON}-V relation appears to reveal gating complexity that has not been previously measured in Hv1 channels. Although both resting-state currents in the R1H mutant (9) and fluorescence signals measured under voltage clamp (29) suggest that VS activation in Hv1 does not proceed in a single gating transition, we previously lacked an experimental approach to directly measure how changes in membrane potential drive gating-charge movement in Hv1. Combined with simultaneous measurements of ionic current and an estimate of the elementary gating valence (z_G), gating-charge measurements provide new insight into the unitary conductance of the G_{AQ} pathway and the

absolute number of functional Hv1 channel subunits in the membrane. Previously, N and γ_{AQ} have been amenable to estimation using current-variance analysis (40). As expected from previous studies (1,27,44,45), neutralization of a highly conserved S4 Arg side chain in Hv1 (R205) decreases the quantity of gating charge per conducting unit (z_G/i). Unexpectedly, however, we find that C-terminal truncation also appears to decrease z_G/i in Hv1 W207A-N214R, suggesting that in addition to its role in stabilizing dimerization (41,46,47), the C-terminus may intimately interact with the voltage-dependent gating machinery. Having the ability to both measure gating current and estimate z_G from the limiting slope on the same protein will enable direct measurement of z_G and γ_{AQ}, allowing researchers to experimentally test hypotheses about VS activation, pH-dependent gating, and H^+ conduction mechanisms in Hv1 that have so far remained mysterious.

pH-dependent gating, which is manifested by an ~40 mV/pH unit shift in the position of the G_{AQ}-V relation, is one of the hallmark biophysical features of Hv1 channels (1,2,7,17). Both V_M and $V_{0.5}$-values determined for I_{TAIL}-V relations are similarly pH-dependent (Fig. 4), indicating that pH_O sensitivity is not perturbed in W207A-N214R, at least under the experimental conditions tested here. At physiological pH (i.e., pH < 8), the W207A single mutant is also sensitive to changes in pH_I (28), suggesting that W207A-N214R probably also senses and transduces changes in ΔpH. pH_O sensitivity in W207A-N214R therefore appears to be similar to WT Hv1 and a large number of other mutants reported previously (1,2,7,11,17,28). This conclusion is reinforced by the observation that apparent z_G estimated from Boltzmann fits to the I_{TAIL}-V and Q_{ON}-V relations is not discernably pH-sensitive between pH_O 5.5 and pH 6.5_O (Fig. 4 *B*).

Although Boltzmann fits to the Q_{ON}-V curves suggest that the unitary gating valence, z_G, is insensitive to changes in pH_O, caution is warranted in the interpretation of z_G-values determined from Boltzmann fits to the data. First, Q_{ON}-V relations in W207A-N214R are evidently complex (Fig. 2 *C*), suggesting that gating-charge movement does not proceed in a single gating step. Boltzmann fitting of G-V curves is known to underestimate z_G, particularly when VS activation requires multiple state transitions and is therefore not well described by a two-state model (35,38). Indeed, z_G estimated using the limiting-slope method in *C. intestinalis* Hv1 (~6 e_0) is two to three times larger than values derived from fits to G_{AQ}-V relations in mammalian Hv1 channels (1,2,14,27,32). We therefore use limiting-slope estimates of z_G for the purpose of calculating channel number and unitary conductance in full-length (6 e_0; i.e., W207A-N214R) and truncated (3 e_0; i.e., W207A-N214R-ΔC) Hv1 channels in this study. Our estimates of N and γ_{AQ} would therefore differ by a factor of only ~2 if values from Boltzmann fits to our data (Table 1) were used.

Although W207A dramatically alters G_{AQ} activation and deactivation kinetics, its effect on estimated unitary conductance was not reported previously (28), and it remains unknown whether mutations of this residue alter the size or structure of the H^+ permeation pathway in Hv1. Resting- and activated-state model and x-ray structures predict that the W207 side chain probably faces away from the hydrated VS central crevice (7–9,32,48–51), suggesting that if W207 mutations alter γ_{AQ}, they probably do so indirectly. On the other hand, the basic side chain of N214R was previously shown to occupy a site that can selectively block outwardly directed H^+ transfer from an intracellular site that lies within the electrical field (9). Because the γ_{AQ} estimated for W207A-N214R (Fig. 3 *B*) is >10-fold smaller than a previous estimate for WT Hv1 (40), we conclude that the N214R side chain probably reduces the amplitudes of both I_{STEP} and I_{TAIL}. Stated differently, the positive charge introduced at the R4 position appears to reduce γ_{AQ} in a voltage-dependent fashion that is reminiscent of pore block by permeant ions in VGCs (52,53).

In summary, we report a method for reliably and reproducibly measuring gating currents in mammalian cells by expressing a human Hv1 double mutant that displays fast activation kinetics and selective block of the outwardly directed ionic H^+ current. I_G in Hv1 displays many of the biophysical features previously reported for other VS-domain proteins, including thermodynamic coupling of VS activation and pore opening. Gating currents also enable new methods for estimating Hv1 unitary conductance and channel number. The ability to directly measure VS activation in Hv1 may be helpful for testing a variety of unresolved hypotheses about the mechanisms of voltage- and pH-dependent gating and H^+ conduction in Hv1. Gating currents are also likely to be useful for addressing fundamental questions about VS activation that are common to Hv1, VSPs, and VGCs. For example, it remains unclear why Hv1 channels are evidently unique among VS-domain proteins in mediating an intrinsic, activated-state G_{AQ}. Gating-current measurements should enable experimental separation of mutagenic effects on VS activation versus pore structure and potentially help to clarify why specific mutations (i.e., D112V in human Hv1) render channels nonfunctional, whereas other substitutions at the same position act mainly to erode H^+ selectivity (11).

SUPPORTING MATERIAL

Four figures are available at http://www.biophysj.org/biophysj/supplemental/S0006-3495(18)30583-6.

AUTHOR CONTRIBUTIONS

V.D.L.R. designed and executed experiments, analyzed results, and prepared figures and tables. I.S.R. designed and executed experiments, analyzed results, prepared figures and tables, and wrote the manuscript.

ACKNOWLEDGMENTS

The authors wish to thank Carlos A. Villalba-Galea for development of data acquisition and analysis software and for many helpful discussions.

This work was supported by NIH R01GM092908 (I.S.R.) and CONACYT postdoctoral fellowship 251376 (V.D.L.R.).

REFERENCES

1. Ramsey, I. S., M. M. Moran, …, D. E. Clapham. 2006. A voltage-gated proton-selective channel lacking the pore domain. *Nature.* 440:1213–1216.
2. Sasaki, M., M. Takagi, and Y. Okamura. 2006. A voltage sensor-domain protein is a voltage-gated proton channel. *Science.* 312: 589–592.
3. Murata, Y., H. Iwasaki, …, Y. Okamura. 2005. Phosphoinositide phosphatase activity coupled to an intrinsic voltage sensor. *Nature.* 435:1239–1243.
4. Yu, F. H., and W. A. Catterall. 2004. The VGL-chanome: a protein superfamily specialized for electrical signaling and ionic homeostasis. *Sci. STKE.* 2004:re15.
5. Bennett, A. L., and I. S. Ramsey. 2017. CrossTalk opposing view: proton transfer in Hv1 utilizes a water wire, and does not require transient protonation of a conserved aspartate in the S1 transmembrane helix. *J. Physiol.* 595:6797–6799.
6. Bennett, A. L., and I. S. Ramsey. 2017. Rebuttal from Ashley L. Bennett and Ian Scott Ramsey. *J. Physiol.* 595:6803.
7. Ramsey, I. S., Y. Mokrab, …, D. E. Clapham. 2010. An aqueous H^+ permeation pathway in the voltage-gated proton channel Hv1. *Nat. Struct. Mol. Biol.* 17:869–875.
8. Wood, M. L., E. V. Schow, …, D. J. Tobias. 2012. Water wires in atomistic models of the Hv1 proton channel. *Biochim. Biophys. Acta.* 1818:286–293.
9. Randolph, A. L., Y. Mokrab, …, I. S. Ramsey. 2016. Proton currents constrain structural models of voltage sensor activation. *eLife.* 5:e18017.
10. Berger, T. K., and E. Y. Isacoff. 2011. The pore of the voltage-gated proton channel. *Neuron.* 72:991–1000.
11. Musset, B., S. M. Smith, …, T. E. DeCoursey. 2011. Aspartate 112 is the selectivity filter of the human voltage-gated proton channel. *Nature.* 480:273–277.
12. Vargas, E., V. Yarov-Yarovoy, …, B. Roux. 2012. An emerging consensus on voltage-dependent gating from computational modeling and molecular dynamics simulations. *J. Gen. Physiol.* 140:587–594.
13. Chanda, B., and F. Bezanilla. 2008. A common pathway for charge transport through voltage-sensing domains. *Neuron.* 57:345–351.
14. Gonzalez, C., H. P. Koch, …, H. P. Larsson. 2010. Strong cooperativity between subunits in voltage-gated proton channels. *Nat. Struct. Mol. Biol.* 17:51–56.
15. De La Rosa, V., A. L. Bennett, and I. S. Ramsay. 2018. Coupling between an electrostatic network and the Zn^{2+} binding site modulates Hv1 activation. *J Gen Physiol.* Published online May 9, 2018. https://doi.org/10.1085/jgp.201711822.
16. Cherny, V. V., D. Morgan, …, T. E. DeCoursey. 2018. Histidine^{168} is crucial for ΔpH-dependent gating of the human voltage-gated proton channel, hHV1. *J Gen Physiol.* Published online May 9, 2018. https://doi.org/10.85/jgp.201711968.
17. Cherny, V. V., V. S. Markin, and T. E. DeCoursey. 1995. The voltage-activated hydrogen ion conductance in rat alveolar epithelial cells is determined by the pH gradient. *J. Gen. Physiol.* 105:861–896.
18. Armstrong, C. M., and F. Bezanilla. 1973. Currents related to movement of the gating particles of the sodium channels. *Nature.* 242:459–461.
19. Almers, W. 1975. Observations on intramembrane charge movements in skeletal muscle. *Philos. Trans. R. Soc. Lond. B Biol. Sci.* 270:507–513.
20. Perozo, E., R. MacKinnon, …, E. Stefani. 1993. Gating currents from a nonconducting mutant reveal open-closed conformations in Shaker K+ channels. *Neuron.* 11:353–358.
21. Ledwell, J. L., and R. W. Aldrich. 1999. Mutations in the S4 region isolate the final voltage-dependent cooperative step in potassium channel activation. *J. Gen. Physiol.* 113:389–414.
22. Long, S. B., E. B. Campbell, and R. Mackinnon. 2005. Voltage sensor of Kv1.2: structural basis of electromechanical coupling. *Science.* 309:903–908.
23. Chowdhury, S., B. M. Haehnel, and B. Chanda. 2014. Interfacial gating triad is crucial for electromechanical transduction in voltage-activated potassium channels. *J. Gen. Physiol.* 144:457–467.
24. Fernández-Marino, A. I., T. J. Harpole, …, B. Chanda. 2018. Gating interaction maps reveal a noncanonical electromechanical coupling mode in the Shaker K^+ channel. *Nat. Struct. Mol. Biol.* 25:320–326.
25. Bezanilla, F., E. Perozo, and E. Stefani. 1994. Gating of Shaker K+ channels: II. The components of gating currents and a model of channel activation. *Biophys. J.* 66:1011–1021.
26. Sakata, S., T. Kurokawa, …, Y. Okamura. 2010. Functionality of the voltage-gated proton channel truncated in S4. *Proc. Natl. Acad. Sci. USA.* 107:2313–2318.
27. Gonzalez, C., S. Rebolledo, …, H. P. Larsson. 2013. Molecular mechanism of voltage sensing in voltage-gated proton channels. *J. Gen. Physiol.* 141:275–285.
28. Cherny, V. V., D. Morgan, …, T. E. DeCoursey. 2015. Tryptophan 207 is crucial to the unique properties of the human voltage-gated proton channel, hHV1. *J. Gen. Physiol.* 146:343–356.
29. Qiu, F., S. Rebolledo, …, H. P. Larsson. 2013. Subunit interactions during cooperative opening of voltage-gated proton channels. *Neuron.* 77:288–298.
30. DeCoursey, T. E. 1991. Hydrogen ion currents in rat alveolar epithelial cells. *Biophys. J.* 60:1243–1253.
31. Villalba-Galea, C. A. 2014. Hv1 proton channel opening is preceded by a voltage-independent transition. *Biophys. J.* 107:1564–1572.
32. Chamberlin, A., F. Qiu, …, H. P. Larsson. 2014. Hydrophobic plug functions as a gate in voltage-gated proton channels. *Proc. Natl. Acad. Sci. USA.* 111:E273–E282.
33. DeCoursey, T. E., and V. V. Cherny. 1997. Deuterium isotope effects on permeation and gating of proton channels in rat alveolar epithelium. *J. Gen. Physiol.* 109:415–434.
34. Tombola, F., M. H. Ulbrich, …, E. Y. Isacoff. 2010. The opening of the two pores of the Hv1 voltage-gated proton channel is tuned by cooperativity. *Nat. Struct. Mol. Biol.* 17:44–50.
35. Bezanilla, F., and C. A. Villalba-Galea. 2013. The gating charge should not be estimated by fitting a two-state model to a Q-V curve. *J. Gen. Physiol.* 142:575–578.
36. Tao, X., A. Lee, …, R. MacKinnon. 2010. A gating charge transfer center in voltage sensors. *Science.* 328:67–73.
37. Lacroix, J. J., H. C. Hyde, …, F. Bezanilla. 2014. Moving gating charges through the gating pore in a Kv channel voltage sensor. *Proc. Natl. Acad. Sci. USA.* 111:E1950–E1959.
38. Chowdhury, S., and B. Chanda. 2012. Estimating the voltage-dependent free energy change of ion channels using the median voltage for activation. *J. Gen. Physiol.* 139:3–17.
39. Ishida, I. G., G. E. Rangel-Yescas, …, L. D. Islas. 2015. Voltage-dependent gating and gating charge measurements in the Kv1.2 potassium channel. *J. Gen. Physiol.* 145:345–358.
40. Cherny, V. V., R. Murphy, …, T. E. DeCoursey. 2003. Properties of single voltage-gated proton channels in human eosinophils estimated by noise analysis and by direct measurement. *J. Gen. Physiol.* 121:615–628.

41. Tombola, F., M. H. Ulbrich, and E. Y. Isacoff. 2008. The voltage-gated proton channel Hv1 has two pores, each controlled by one voltage sensor. *Neuron.* 58:546–556.

42. Musset, B., V. V. Cherny, …, T. E. DeCoursey. 2008. Detailed comparison of expressed and native voltage-gated proton channel currents. *J. Physiol.* 586:2477–2486.

43. Villalba-Galea, C. A., W. Sandtner, …, F. Bezanilla. 2008. S4-based voltage sensors have three major conformations. *Proc. Natl. Acad. Sci. USA.* 105:17600–17607.

44. Seoh, S. A., D. Sigg, …, F. Bezanilla. 1996. Voltage-sensing residues in the S2 and S4 segments of the Shaker K+ channel. *Neuron.* 16:1159–1167.

45. Aggarwal, S. K., and R. MacKinnon. 1996. Contribution of the S4 segment to gating charge in the Shaker K+ channel. *Neuron.* 16:1169–1177.

46. Koch, H. P., T. Kurokawa, …, H. P. Larsson. 2008. Multimeric nature of voltage-gated proton channels. *Proc. Natl. Acad. Sci. USA.* 105:9111–9116.

47. Lee, S. Y., J. A. Letts, and R. Mackinnon. 2008. Dimeric subunit stoichiometry of the human voltage-dependent proton channel Hv1. *Proc. Natl. Acad. Sci. USA.* 105:7692–7695.

48. Okuda, H., Y. Yonezawa, …, Y. Fujiwara. 2016. Direct interaction between the voltage sensors produces cooperative sustained deactivation in voltage-gated H+ channel dimers. *J. Biol. Chem.* 291:5935–5947.

49. Takeshita, K., S. Sakata, …, A. Nakagawa. 2014. X-ray crystal structure of voltage-gated proton channel. *Nat. Struct. Mol. Biol.* 21:352–357.

50. Li, Q., R. Shen, …, E. Perozo. 2015. Resting state of the human proton channel dimer in a lipid bilayer. *Proc. Natl. Acad. Sci. USA.* 112:E5926–E5935.

51. Kulleperuma, K., S. M. Smith, …, R. Pomès. 2013. Construction and validation of a homology model of the human voltage-gated proton channel hHV1. *J. Gen. Physiol.* 141:445–465.

52. Woodhull, A. M. 1973. Ionic blockage of sodium channels in nerve. *J. Gen. Physiol.* 61:687–708.

53. Hille, B., and W. Schwarz. 1978. Potassium channels as multi-ion single-file pores. *J. Gen. Physiol.* 72:409–442.

Biophysical Journal, Volume *114*

Supplemental Information

Gating Currents in the Hv1 Proton Channel

Victor De La Rosa and Ian Scott Ramsey

SUPPLEMENTARY FIGURE LEGENDS

Supplementary Figure 1. Effect of varying voltage prepulse duration on I_{TAIL}-V and Q_{ON}-V relations in W207A-N214R.

A) The absolute value of I_{TAIL} measured at V_{TAIL} = -90 mV after V_{STEP} for the indicated duration to voltages between -60 mV and +50 mV (V_{STEP}: -60 mV, red circles; -50 mV, orange circles; -40 mV, yellow circles; -30 mV, olive circles; -20 mV, green circles; -10 mV, aqua circles; 0 mV, cyan circles; +10 mV, blue circles; +20 mV, indigo circles; +30 mV, violet circles; +40 mV, black circles; +50 mV, gray circles) in a representative cell expressing W207A-N214R is shown. Solid lines represent fits to a single exponential function (-60 mV: τ = 102.5 ms, red line; -50 mV: τ = 155.6 ms, orange line; -40 mV, τ = 301.3 ms, yellow line; -30 mV, τ = 355.3 ms, olive line; -20 mV, τ = 236.4 ms, green line; -10 mV, τ = 153.2 ms, aqua line; 0 mV, τ = 102.4 ms, cyan line; +10 mV, τ = 73.3 ms, blue line; +20 mV, τ = 52.9 ms, indigo line; +30 mV, τ = 37.4 ms, violet line; +40 mV, τ = 27.1 ms, black line; +50 mV, τ = 21 ms, gray line). Note that the Legend applies to panels A and B.

B) Q_{ON} in the same cell as shown in panel **A** is measured at V_{STEP} = +100 mV after V_{PP} for the indicated duration to voltages between -70 mV and +40 mV (V_{PP}: -70 mV, magenta circles; -60 mV, red circles; -50 mV, orange circles; -40 mV, yellow circles; -30 mV, olive circles; -20 mV, green circles; -10 mV, aqua circles; 0 mV, cyan circles; +10 mV, blue circles; +20 mV, indigo circles; +30 mV, violet circles; +40 mV, black circles). Solid lines represent fits to a single exponential function (-70 mV: $\tau = 2.4 \times 10^8$ ms, magenta line;-60 mV: τ = 407.6 ms, red line; -50 mV: τ = 333.5 ms, orange line; -40 mV, τ = 365.5 ms, yellow line; -30 mV, τ = 273.1 ms, olive line; -20 mV, τ = 161.1 ms, green line; -10 mV, τ = 105.4 ms, aqua line; 0 mV, τ = 64.3 ms, cyan line; +10 mV, τ = 43.1 ms, blue line; +20 mV, τ = 28.7 ms, indigo line; +30 mV, τ = 20.9 ms, violet line; +40 mV, τ = 19.5 ms, black line).

C, D) Linear leak-subtracted I_{TAIL}-V (**C**) or Q_{ON}-V (**D**) relations are normalized to their respective maxima and plotted in function of V_{STEP} or V_{PP} duration (50 ms, red circles; 100 ms, blue triangles; 200 ms, magenta triangles; 500 ms, green diamonds; 1000 ms, indigo triangles; 2000 ms, violet triangles).

E, F) $V_{0.5}$ (**E**) and z_G (**F**) values determined from Boltzmann fits to I_{TAIL}-V (black stars; see panel **C**) or Q_{ON}-V (red stars; see panel **C**) relations are shown in function of V_{PP} (for Q_{ON}) or V_{STEP} (for I_{TAIL}) duration. Solid lines in panel **E** represent fits to a double exponential function of the form $V_{0.5} = V_{0.5(0)} + A_1 \cdot e^{t/\tau 1} + A_2 \cdot e^{t/\tau 2}$ (red line: Q_{ON}: $V_{0.5(0)}$ = -44.7 mV, A_1 = 136 mV, $\tau 1$ = 20.6 ms, A_2 = 29.8 mV, $\tau 2$ = 310.4 ms; black line, I_{TAIL}: $V_{0.5(0)}$ = -34.4 mV, A_1 = 142.1 mV, $\tau 1$ = 21.3 ms, A_2 = 50.6 mV, $\tau 2$ = 211.8 ms). Solid lines in panel **F** represent fits to a single exponential function of the form $z_{\square} = z_{G(0)} + A \cdot e^{t/\tau 1}$ (red line: Q_{ON}: $z_{G(0)}$ = 2.3 e_0, A = -1.5 e_0, τ = 260.3 ms; black line, I_{TAIL}: $z_{G(0)}$ = 3.2 e_0, A = -2.3 e_0, τ = 261.5 ms).

Supplementary Figure 2. Steady-state I_{STEP}-V relations in W207A-N214R.

A, B) Representative currents elicited by the indicated double-pulse voltage protocols (**A**: to measure I_G at +140 mV; **B**: to measure I_{TAIL} at -90 mV) in a cell expressing R205A-N214R are shown. ***Inset*** shows outward transient current attributed to I_G at higher resolution.

C) Normalized mean (± SEM) I_{TAIL}-V and Q_{ON}-V relations expressing R205A-N214R are shown (n = 3 cells). Mean $V_{0.5}$, z_G and V_M values are reported in Table 1.

D) Plots of maximal Q_{ON} ($Q_{ON\ max}$) vs. maximal I_{TAIL} ($I_{TAIL\ max}$) measured in individual cells expressing R205A-N214R (filled red circles), W207A-N214R data (Figure 3) is shown for comparison. Linear fit to the data: slope 2.5 pC/nA; R^2= 0.93.

E) The number of channels (N) is calculated as described in Fig. 3. Linear fit to the data yield an estimate of the unitary conductance.

Supplementary Figure 3.

A) Representative currents in a representative cell expressing W207A-N214R-ΔC elicited by the indicated voltage step protocol (V_{HOLD} = -80 mV; V_{STEP} = 50 mV for 0 to 200 ms in 5 ms intervals; V_{TAIL} = -90 mV) are shown.

B) I_{TAIL} activation time courses determined from experiments like that shown in panel **A** are measured over the range of V_{STEP} indicated by the legend are shown. Data are fit to a single exponential without a delay (see *Methods*).

C) I_{STEP} elicited by a voltage step to +50 mV (black line; data from panel **A**) is shown together with the fitted I_{TAIL} activation time course (red line; data from panel **B**) scaled to the amplitude of the steady-state I_{STEP}.

D) I_{STEP} at various V_{STEP} is determined after subtraction of a scaled exponential fit to the I_{TAIL} activation timecourse measured at the indicated V_{STEP}, as shown in panel **C** for data at +50 mV.

E) Q_{ON}-V relation resulting from integrating the subtracted I_{STEP} records (panel **D**) is shown (solid black squares). A Boltzmann fit of the data yields parameters ($V_{0.5}$ = -33.5 mV; z_G = 1.81 e_0) that are similar to values reported for the Q_{ON}-V relation in W207A-N214R obtained without subtraction of the fitted and scaled I_{TAIL} timecourse (Table 1).

F) The decaying phase of subtracted I_{STEP} records (panel **D**) are fit to a single exponential function without a delay (see *Methods*) and the fitted time constant (τ_{DEACT}) from is shown in function of V_{STEP} (open black squares).

Supplementary Figure 4.

A, B) Representative currents in a cell expressing W207A-N214R are elicited by the indicated double-pulse voltage protocols at pH_O 6.5 (**A**) and pH_O 5.5 (B). I_G is measured at +50 mV (A) or +90 mV (B) and I_{TAIL} (square symbols) is measured at -90 mV (A) or -50 mV (B).

C) I_{STEP}-V relations from n = 9 (pH_O 6.5, open black squares) or n = 4 (pH_O 5.5, filled red squares) experiments are linear leak-subtracted and normalized to the amplitude of the maximal inward current; the mean (± SEM) values are plotted in function of V_{STEP}.

Figure S1

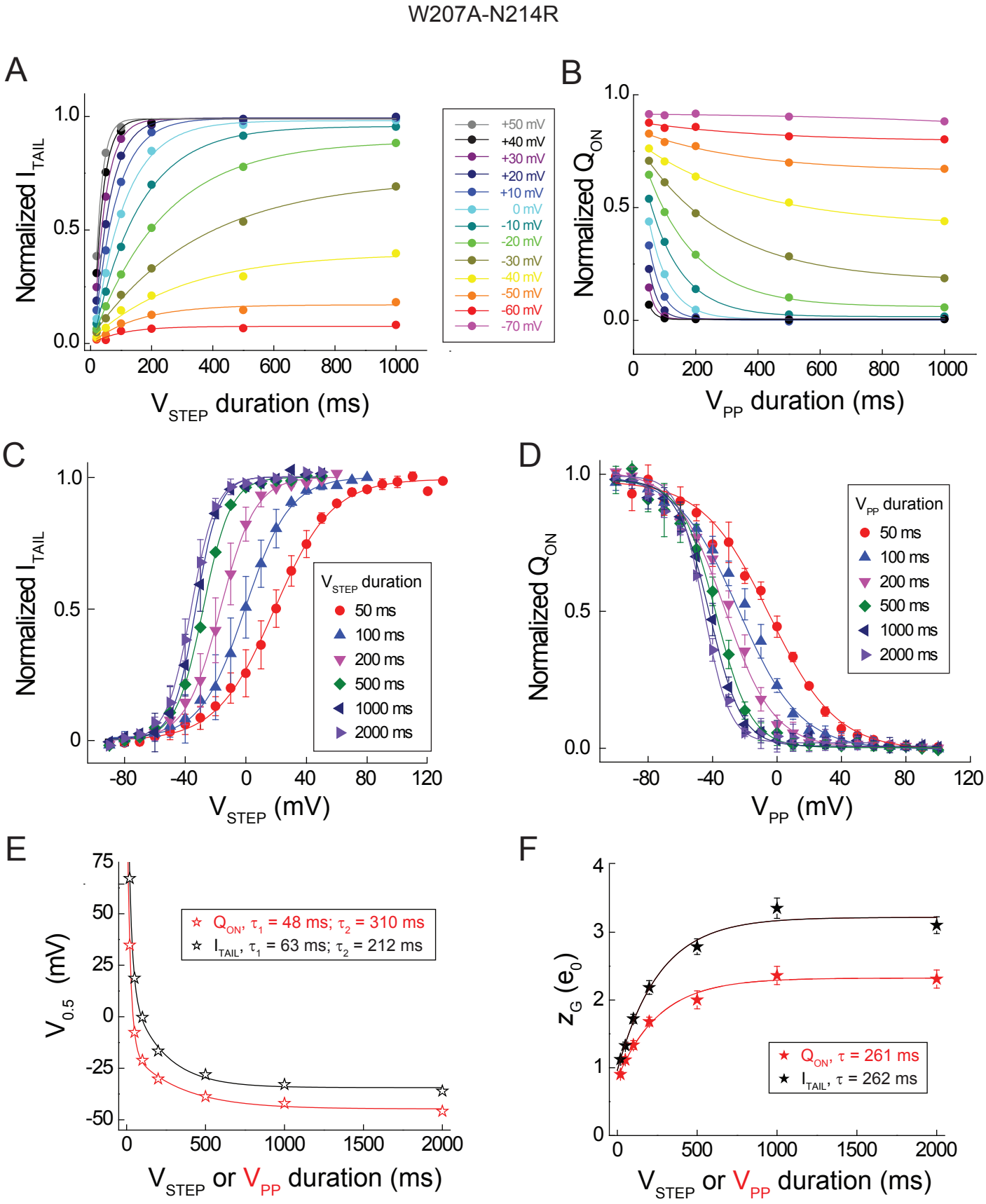
W207A-N214R
A
Normalized I_{TAIL}
V_{STEP} duration (ms)
+50 mV
+40 mV
+30 mV
+20 mV
+10 mV
0 mV
-10 mV
-20 mV
-30 mV
-40 mV
-50 mV
-60 mV
-70 mV
B
Normalized Q_{ON}
V_{PP} duration (ms)
C
Normalized I_{TAIL}
V_{STEP} (mV)
V_{STEP} duration
50 ms
100 ms
200 ms
500 ms
1000 ms
2000 ms
D
Normalized Q_{ON}
V_{PP} (mV)
V_{PP} duration
50 ms
100 ms
200 ms
500 ms
1000 ms
2000 ms
E
$V_{0.5}$ (mV)
Q_{ON}, τ_1 = 48 ms; τ_2 = 310 ms
I_{TAIL}, τ_1 = 63 ms; τ_2 = 212 ms
V_{STEP} or V_{PP} duration (ms)
F
z_G (e_0)
Q_{ON}, τ = 261 ms
I_{TAIL}, τ = 262 ms
V_{STEP} or V_{PP} duration (ms)

Figure S2

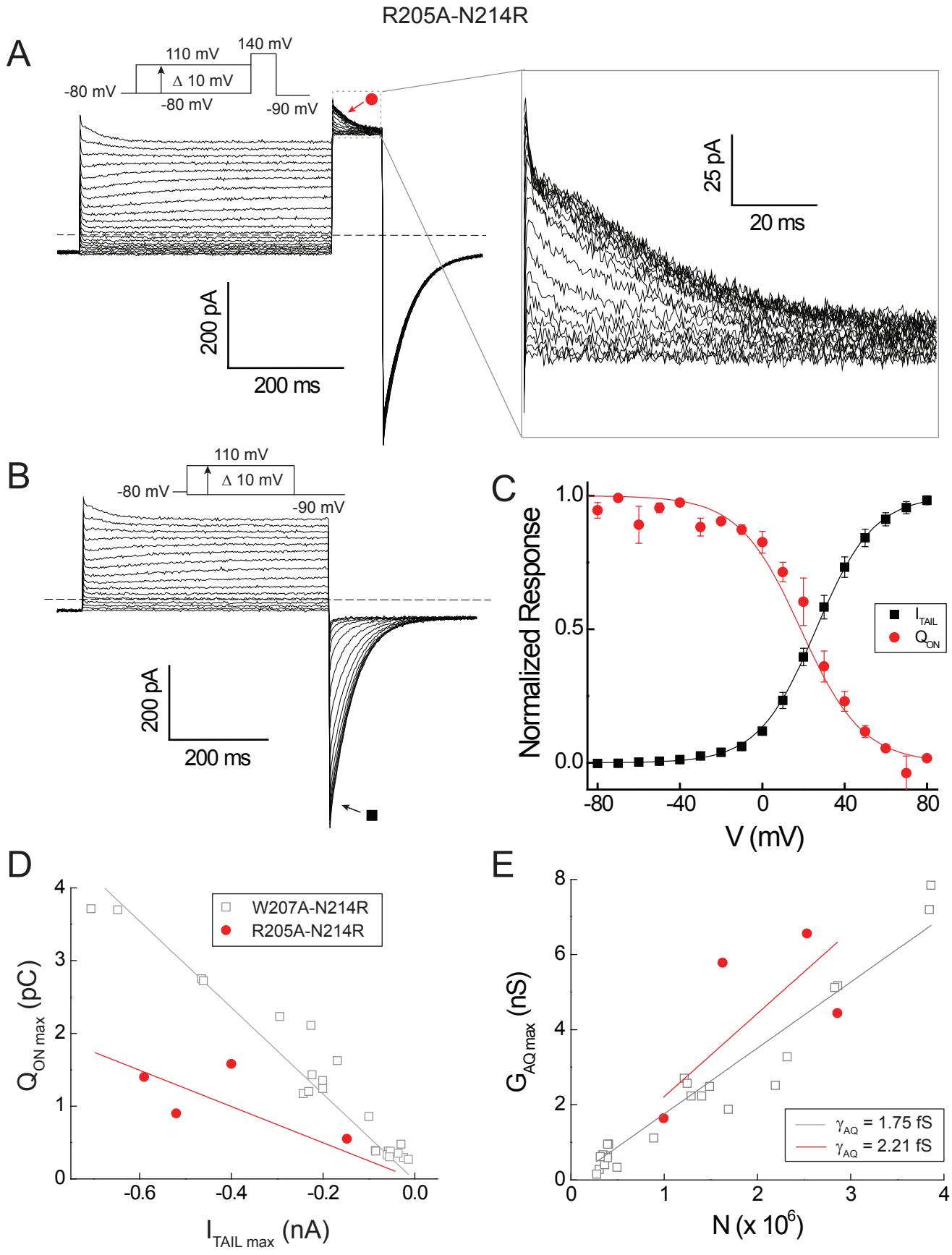
R205A-N214R
A
110 mV
140 mV
Δ 10 mV
-80 mV
-80 mV
-90 mV
200 pA
200 ms
25 pA
20 ms
B
110 mV
Δ 10 mV
-80 mV
-90 mV
200 pA
200 ms
C
Normalized Response
1.0
0.5
0.0
-80
-40
0
40
80
V (mV)
I_TAIL
Q_ON
D
W207A-N214R
R205A-N214R
Q_ON max (pC)
I_TAIL max (nA)
E
G_AQ max (nS)
N (x 10^6)
γ_AQ = 1.75 fS
γ_AQ = 2.21 fS

Figure S3

W207A-N214R-ΔC

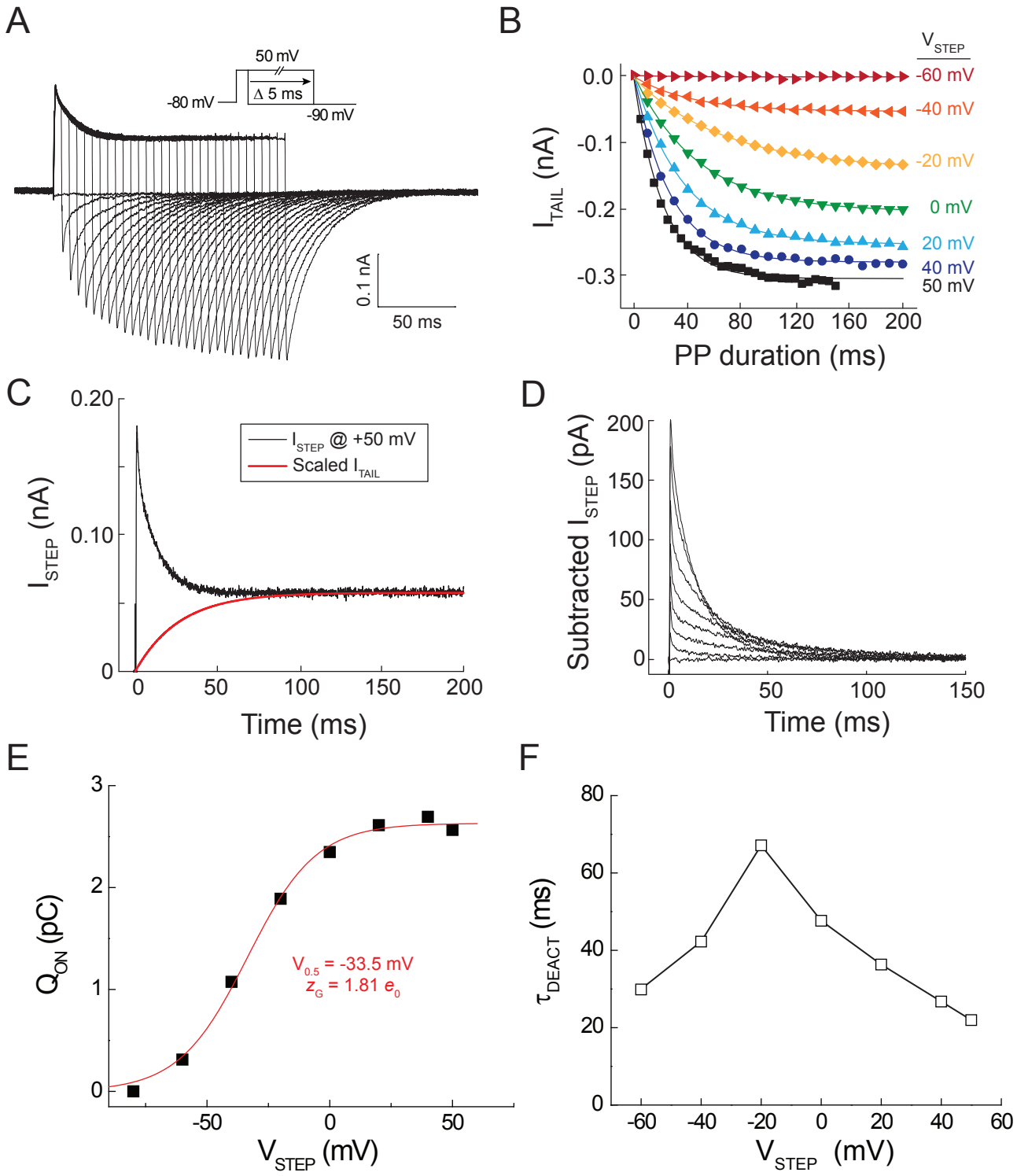

Figure S4

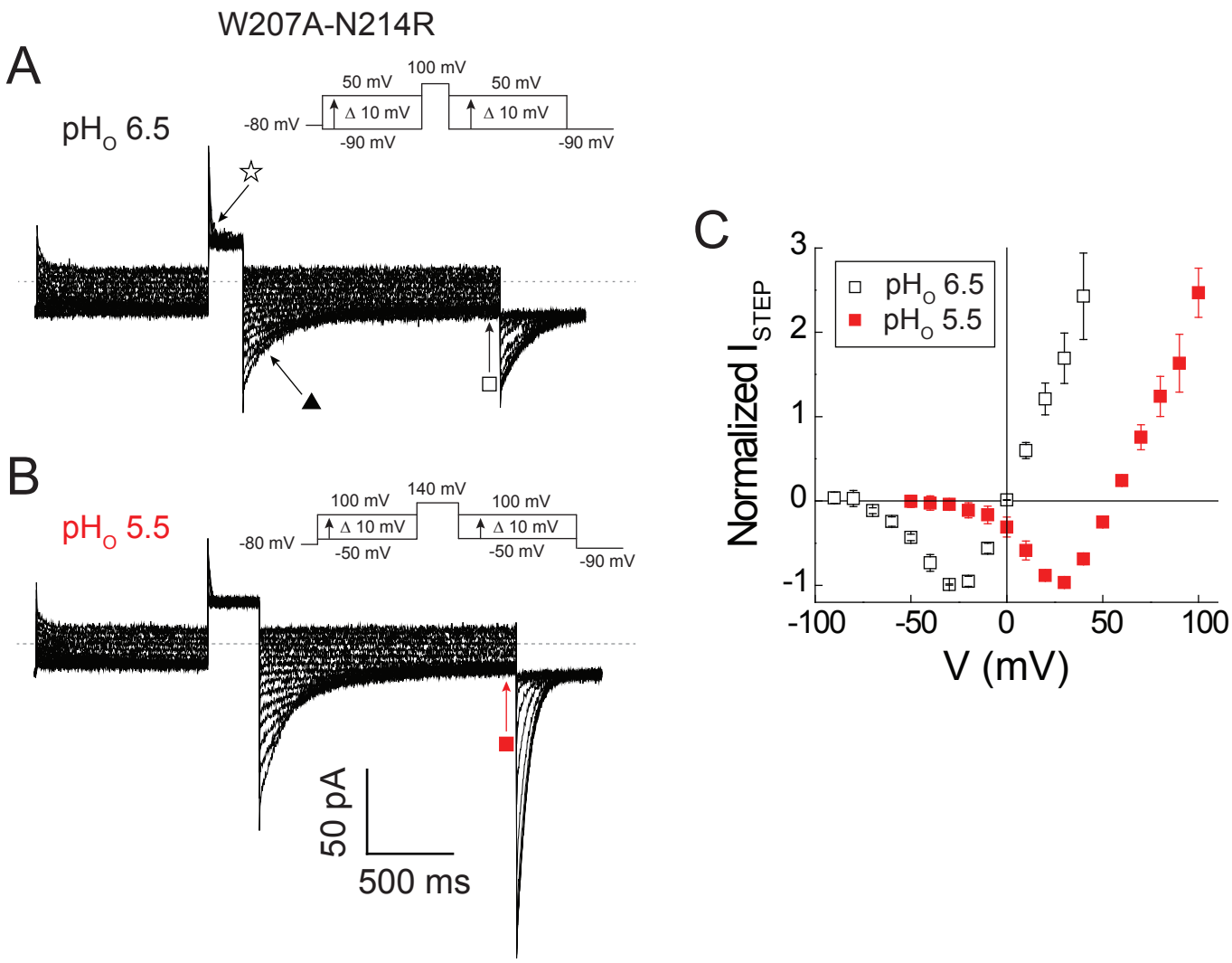
W207A-N214R
A
pH$_O$ 6.5
100 mV
50 mV
50 mV
Δ 10 mV
Δ 10 mV
-80 mV
-90 mV
-90 mV
B
pH$_O$ 5.5
140 mV
100 mV
100 mV
Δ 10 mV
Δ 10 mV
-80 mV
-50 mV
-50 mV
-90 mV
50 pA
500 ms
C
Normalized I$_{STEP}$
pH$_O$ 6.5
pH$_O$ 5.5
3
2
1
0
-1
-100
-50
0
50
100
V (mV)